Wettability and hydrolytic stability of 3-aminopropylsilane coupling agent and phenol-urea-formaldehyde binder on silicate surfaces and fibers

Okhrimenko, D. V.; Budi, A.; Ceccato, M.; Johansson, D. B.; Lybye, Dorthe; Bechgaard, Klaus; Stipp, S. L.S.

Published in:
Polymer Degradation and Stability

Link to article, DOI:
10.1016/j.polymdegradstab.2020.109431

Publication date:
2021

Document Version
Peer reviewed version

Wettability and hydrolytic stability of 3-aminopropylsilane coupling agent and phenol-urea-formaldehyde binder on silicate surfaces and fibers

D.V. Okhrimenko[1,*], A. Budi[2], M. Ceccato[3,4], D.B. Johansson[1],
D. Lybye[1], K. Bechgaard[5,†], S.L.S. Stipp[6]

[1]ROCKWOOL International A/S, Hovedgaden 584, 2640 Hedehusene, Denmark.
[2]Institute for Frontier Materials, Deakin University, Geelong, VIC 3216, Australia.
[3]Interdisciplinary Nanoscience Center (iNANO), Aarhus University, Aarhus 8000, Denmark
[4]Department of Chemistry, Aarhus University, Aarhus 8000, Denmark
[5]Department of Chemistry, University of Copenhagen, 2100 Copenhagen Denmark
[6]Department of Physics, Danish Technical University, 2800 Kongens Lyngby, Denmark
[†] - deceased

Corresponding Author
*Phone: +45 46 55 81 30. E-mail: denis.okhrimenko@rockwool.com

Abstract
The stability of phenol-urea-formaldehyde (PUF) binder and 3-aminopropylsilane (APS) on composite silicate materials (fibers and wafers) was studied with surface sensitive techniques (X-ray photoelectron spectroscopy (XPS) and streaming potential) through a wide range of humidity and temperature and *ab initio* modelling complemented the results. Behavior was compared for wettability properties, determined by vapor adsorption and contact angle analysis. APS and PUF, deposited on the silicate surfaces, decrease surface energy and wettability but water adsorption remains high, facilitating hydrolytic decomposition of the composite material. Deposited APS is unstable at T>50 °C and 75% RH, while PUF is less sensitive to high humidity and temperature. Molecular dynamics confirmed APS sensitivity to humidity. Water adsorption and surface energy decrease, and material stability increases when a hydrophobization agent is applied to APS/PUF treated surfaces. The direct correlation between wettability and stability of PUF/APS/fiber composites can contribute in designing new materials with controlled hydrophobic properties.

KEWWORDS: Amorphous materials, Coupling agents, Fibre/matrix bond, Interface, Surface treatments.

1. Introduction

Aminosilane treatment of silica and silicate surfaces is widely used in industry, construction, biomaterials and medical applications, to improve adhesion of polymers and durability of composite materials. Better understanding of the complex interactions between inorganic solids, water and organic adsorbates will find particular application in tailoring new functional materials with controlled wetting and ageing properties. One industrial example is production of glass-polymer composite materials [1], such as stone wool. Stone wool is composed of fibers which are produced from natural rock material, such as basalt, olivine, dolomite, diabase etc. Fibers have amorphous glassy structure and joined together by organic binder, which is often thermosetting resin. In this work, we have investigated the interaction of stone wool fibers, where 3-aminopropylsilane (APS) enhances adhesion between the solid [2, 3] and the phenol-urea-formaldehyde (PUF) resin [4]. APS reacts with silicate surfaces, through $–Si(OH)_3$, and with PUF, through amine, $–NH_2$, creating sites in the fiber material, where fibers bonded with each other. This creates the necessary mechanical properties and can be used to design the form of the fiber material. During exposure to extreme atmospheric conditions however, such as high temperature and humidity, the mechanical properties of the fiber materials can deteriorate. Weakening mechanical properties can be explained by hydrolysis of the bonds between the APS and the silicate surface [5], between the APS and the PUF

binder, by degradation of the PUF binder matrix itself [6] or by dissolution of the fiber top surface layer [7]. Determining the mechanism gives clues for improved product design but more important, it promotes understanding of a range of applications, across several disciplines.

Min et al., 2012 [8] showed that APS deposited on silica wafers or glass is stable for several weeks under N_2 gas at –18 °C, but at ambient conditions, amide species form. Vandenberg et al., 1991 [9] and Kim et al., 2008 [10] demonstrated instability of freshly prepared APS layers in water but demonstrated increased stability and APS swelling in water if the samples were cured at high temperature. Preparation of APS layers at elevated temperature also leads to higher hydrolytic stability than preparation at room temperature [11]. Smith and Chen, 2008 [12] and Zhu et al., 2011 [13] confirmed with ellipsometry, that APTES layers are unstable in water at 40 °C. Similar results were observed for APS treated silicates, aged in a water bath at elevated temperature by Zafar et al., 2012 [14] and Okhrimenko et al., 2017 [5] and at room temperature by Yadav et al., 2014 [15]. Etienne and Walcarius, 2003 [16] showed that APS layers stability is pH dependent and decomposition happens even in buffered neutral solutions, but APS monolayers are stable in organic solvents, such as dimethyl sulfoxide [17]. However, little is known about APS interface stability in combination with polymers in composite materials.

Hydrolytic stability for PUF and PUF related polymers, such as urea-formaldehyde and phenol-formaldehyde, has been monitored by formaldehyde release [18-23] as well as with surface sensitive techniques [6, 24]. From the literature, one can conclude that water plays an essential role in APS layers and PUF stability. Silicate surfaces are hydrophilic, so organo-silane deposition decreases wettability [25-27]. Water contact angle, measured on APS treated silica, quartz and silicates, can vary from 45 to 58 °, depending on pH in the water droplet [28] and from 56 to 64° depending on the APS solution concentration used for treatment [29]. However, these contact angles indicate that surfaces remain hydrophilic and water wet. Grafting of other silanes, with hydrophobic properties [30, 31], together with APS and creation of dual layers is possible [32] to increase water repellency [33] and stability [34]. Such layers have a higher water contact angle, and this can be controlled by the hydrocarbon chain length of the additive [35]. However, for large scale production, simple and cheaper methods for decreasing water wettability of the silicate materials are necessary.

The purposes of our work were 1) to investigate the wettability of silica and silicate surfaces treated with APS coupling agent and PUF binder, 2) to connect wettability properties of these composite materials with their behavior during ageing over a wide range of temperature and humidity, 3) to elucidate hydrolytic degradation mechanism of the PUF-APS-silicate interface and identify chemical bonds that are mostly subjected for hydrolysis. For that APS was deposited from aqueous solution onto model surfaces (silica and stone wool fiber melt wafers) and untreated stone wool fibers. Wettability was monitored by change in contact angle and vapor adsorption and we compared wettability and ageing of the obtained materials with similar industrial fiber products containing a hydrophobic agent. We also investigated wettability and ageing of industrial stone wool fibers, where PUF binder had been applied. Ageing was done over a range of temperature and relative humidity (RH) for 7, 14, 21 and 28 days, and some samples were treated in water bath at 80 °C for 3 hours, for comparison. The choice of conditions reflects ageing tests and storage conditions widely used in industry (usually from room temperature to 70 °C and from 55% to 97% RH). The samples were analyzed using streaming potential and X-ray photoelectron spectroscopy (XPS). Based on these results, the rate of surface coverage decomposition under various ageing conditions were compared.

2. Experimental details

2.1. Materials

Chemically polished (final surface roughness <2 Å) boron doped silicon wafers (Silicon Material Inc.) with thickness 675 ± 15 μm and 100 nm depth wet oxidized layer were used as 10 x 10 squares. They are referred to in the text as **U-Si** (**u**ntreated **si**lica wafers). **U**ntreated **s**tone **w**ool **m**elt wafers (10×10 mm square samples, **U-SWM**) were produced by ROCKWOOL International A/S. Prior to silanization, wafers were subjected to UV-ozone cleaning for 30 min and rinsing with MilliQ (MQ, specific resistance >18 MOhm•cm) water and dried in a N_2 gas stream. For minimizing organic contamination of the stone wool fibers (**U-SWF**), they were UV-ozone cleaned for 60 min.

Surfaces were silanized with aqueous solution (4 vol. %) of 3-aminopropyltriethoxysilane (APS, Momentive, SILQUEST A-1100), which was prepared 12 hours before using to achieve hydrolyzation of the $Si(OEt)_3$ bonds. Wafer were kept in APS solution for 24 hours and no stirring was applied. After silanization, we rinsed wafer using small amount of MQ water and after that dried samples in a N_2 gas stream. To complete silanization, samples were cured at 110 °C for 20 minutes. The obtained APS treated silica wafers are referred to as **Si-APS** and the treated stone wool melt wafers are called **SWM-APS.**

We used **u**ntreated **s**tone **w**ool **f**ibers (**U-SWF**) produced by ROCKWOOL International A/S and we also silane-treated them. For that, a slurry of 10 g of fibers mixed with 5 ml of 0.4 vol. % APS solution was prepared and heated to 90 °C for 10 minutes. To complete silanization, we further increased the temperature to 160 °C for another 15 minutes. This sample is referred to as **SWF-APS**. Wafers and fibers preparation and silanization are described earlier in our previous paper [5]. We also used stone wool fibers that were treated with APS in the standard manufacturing process at ROCKWOOL International A/S. These fibers also contain significant amounts of oil used for keeping dust levels low in the factory and to increase the hydrophobic properties of the material. These samples are referred to as **SWF-APS-Oil**. In addition, we tested stone wool fibers that had only been treated with oil (**SWF-Oil**) and a final stone wool product that had been treated with phenol-urea-formaldehyde (PUF) binder, oil and APS (**SWF-PUF**). All of these samples were produced at ROCKWOOL International A/S at different production facilities.

The fluids used for surface energy determination included: MQ water, diiodomethane (Sigma-Aldrich, ReagentPlus®, 99%, contains copper as stabilizer), n-dodecane (Fluka AG, 99.3%) and absolute ethanol (Sigma-Aldrich, >99.8%).

2.2. Ageing

After silanization, the silica and fiber melt wafers (Si-APS and SWM-APS) and stone wool fibers (SWF-APS) were aged in a climate chamber over a series of relative humidity (RH) and temperature conditions, together with the fiber materials (SWF-Oil, SWF-APS-Oil and SWF-PUF) obtained from ROCKWOOL International A/S. We tested at several conditions: 1) room temperature and 55 % RH; 2) room temperature and 97 % RH; 3) 50 °C and 95 % RH; 4) 70 °C and 75% RH; 5) 70 °C and 91% RH. Samples were investigated using several techniques, in the pristine state as well as after ageing for 7, 14, 21 and 28 days. For comparison and reference, we aged some samples at an accelerated rate, in a water bath at 80 °C for 3 hours.

2.3. Surface chemistry (X-ray photoelectron spectroscopy, XPS) and charge (streaming potential) analysis

To investigate surface chemistry and charge of wafer and fiber samples, we performed XPS experiments on a Kratos Axis UltraDLD system and streaming potential measurements were made using an Anton Paar SurPass Electrokinetic Analyzer. Detailed description of the methods can be found in our previous publication [5]. Here, we briefly sum up the details. XPS analysis was performed under ultrahigh vacuum (5•10-9 torr) with a monochromatic AlKα X ray source (hν = 1486.6 eV, power = 150 W). For the survey scans pass energy was set to 160 eV and step size to 0.3

eV while for high resolution scans (C 1s and N 1s) pass energy 10 eV and step size of 0.1 eV were used. Spectra were calibrated using C 1s peak at 285.0 eV, then fitted with Shirley background correction and analyzed with CasaXPS software.

Streaming potential analysis was performed using adjustable gap cell with a 100 μm slit channel between wafers and using cylindrical cell for fibers (0.5.g) Electrolyte solution (1 mM NaCl) was pushed through the cells until pressure raised to 300 mbar. Zeta potential was measured in a pH range 5 < pH < 9.2 and calculated using an approximation of Helmholtz-Smoluchowski equation for fiber samples:

$$\zeta = \frac{dU}{dp} \times \frac{\eta}{\varepsilon \times \varepsilon_0} \times \kappa_B \quad (1)$$

and Helmholtz-Smoluchowski equation for wafer samples:

$$\zeta = \frac{dI}{dp} \times \frac{\eta}{\varepsilon \times \varepsilon_0} \times \frac{L}{A} \quad (2)$$

where ζ represents zeta potential; dU/dp and dI/dp, the slope of the streaming potential and current versus pressure; η, electrolyte viscosity; ε_0, vacuum permittivity; ε, dielectric constant of the electrolyte; κ_B, specific electrical conductivity of the electrolyte outside the capillary system; L, length of the slit channel (10 mm) and A, its cross section. Changes of theses parameters during measurements are controlled automatically by software. The isoelectric point, IEP, was found at pH where the ζ potential was zero, i.e.where the net surface charge is zero. This value can be used as a characteristic value for the surface. We have used IEP analysis previously, to determine the stability of APS layers on wafers and fibers [5] and of PUF binder on fibers [6].

2.4. Wettability determination

We measured contact angles for wafers and vapor adsorption for fibers. The water-diiodomethane pair was used to estimate the surface energy of the wafers and water contact angle in n-dodecane was used to determine the interfacial surface energies and thus preferential wettability of the wafers. For vapor adsorption, we used vapors of MQ water and absolute ethanol. The dispersive and polar components of surface energy (tension) for all of the liquids are summarized in Table 1.

Table 1. Surface energy (tension) of the liquids used for solid surface energy determination [36].

Liquid	Surface energy (tension), mJ/m^2 (mN/m)		
	Dispersive, γ_L^d	Polar, γ_L^p	Total, γ_L
Water	21.8	51	72.8
Diiodomethane	50.8	0	50.8
n-Dodecane	25.4	0	25.4
Ethanol	18.8	2.6	21.4

2.4.1. Contact angle determination

The contact angle measurements were taken from photographs made using a DNT DigiMicro Profi USB camera and captured using the MicroCapturePro software. The volume of the droplets was approximately 1 μL and measurements were made in duplicate on both sides of the droplet. Contact angles were determined using ImageJ software and average contact angle was calculated.
The work of adhesion for the liquids was determined using the measured contact angle and the equation:

$$W_A = \gamma_L(cos\theta + 1), \quad (3)$$

where W_A denotes work of adhesion; γ_L, total surface tension of the liquid; θ, contact angle. When work of adhesion of two liquids with known dispersive and polar components is estimated, it is possible to calculate the dispersive and polar components of the solid surface energy using Owens-Wendt approach (1969) [37]:

$$W_A = 2(\gamma_S^d \gamma_L^d)^{1/2} + 2(\gamma_S^p \gamma_L^p)^{1/2}, \quad (4)$$

where $\gamma_S{}^d$ and $\gamma_S{}^p$ represent the dispersive and polar components of the solid surface energy and $\gamma_L{}^d$ and $\gamma_L{}^p$ represent the dispersive and polar components of the liquid surface energy (Table 1). When dispersive and polar components of the solid surface are calculated, the total surface energy of the solid can be estimated as a sum of the two components (Fowkes, 1963) [38]:

$$\gamma_S = \gamma_S^d + \gamma_S^p. \quad (5)$$

When γ_S is known, the solid-water interfacial surface tension can be determined from the modified Young equation:

$$\gamma_{SW} = \gamma_S - \gamma_W cos\theta_1, \quad (6)$$

where γ_{SW} denotes interfacial surface tension between solid and water; γ_S, total surface energy; γ_W, surface tension of water and θ_1, the water contact angle. When the water contact angle is measured in n-dodecane, it is also possible to estimate the n-dodecane-solid interfacial surface tension, γ_{SO}:

$$\gamma_{SO} = \gamma_{SW} - \gamma_{WO} cos\theta_2, \quad (7)$$

where γ_{SO} denotes interfacial surface tension between solid and n-dodecane; γ_{SW}, interfacial surface tension between solid and water; γ_{WO}, the interfacial surface tension between water and n-dodecane (56.2 mJ/m^2) [39] and θ_2, the water contact angle on the solid in n-dodecane. If the difference between γ_{SW} and γ_{SO}, is negative, then the solid surface is water wet and if this difference is positive, the surface is oil wet.

2.4.2. Gas and vapor adsorption

To determine the surface area of the fiber samples, we used nitrogen adsorption on a Quantachrome Autosorb-1 Sorption Analyser. The samples were first degassed by heating to 80 °C in vacuum ($<10^{-3}$ torr) for 24 hours. The surface area was determined from the nitrogen adsorption isotherm in the relative pressure range $0.1 < P/P_0 < 0.3$ at liquid nitrogen temperature (77 K), using the BET equation [40]. For all samples, the BET plots were linear in the relative pressure range examined and the BET constant, C, was >50, confirming the validity of the BET equation.

Vapor adsorption experiments were performed on the same Quantachrome Autosorb-1 Sorption Analyser, using switched to vapor adsorption mode and following procedure described earlier in previous paper [41]. As probe molecules, we chose MQ water and absolute ethanol. The amount of adsorbed water and ethanol was determined in the interval $5 \cdot 10^{-3} \leq P/P_0 \leq 0.9$ and was normalized to the surface area determined with nitrogen adsorption. The analyses were made at constant temperature at 5, 12, 20 °C for water and 5, 20 and 30 °C for ethanol.

Using isotherms that were measured at several temperatures, the amount of energy involved in the sorption process, Q_{st}, was determined from the slope of adsorption isosteres, with the Clausius-Clapeyron equation:

$$Q_{st} = -R \left(\frac{\partial \ln(P)}{\partial (\frac{1}{T})} \right)_\theta, \quad (8)$$

where P represents the equilibrium pressure of the adsorbate and T stands for the absolute temperature and R is ideal gas constant. Q_{st} is also known as isosteric heat of adsorption or the enthalpy of sorption. The subscript, θ, shows that the calculations were made for a constant adsorbed amount.

Following the Schlangen et al. 1994 [42] approach, surface pressure, π_{sv}, was calculated at 20 °C:

$$\pi_{SV} = \gamma_S - \gamma_{SV} = RT \int_{P=0}^{P} \Gamma(P) d ln \frac{P}{P_0}, \quad (9)$$

where γ_S represents surface energy of the solid toward vacuum, γ_{sv}, the interfacial surface energy of the solid in contact with the adsorbate vapor and Γ stands for the adsorbed vapor amount. Because of high amounts of vapor adsorbed by the fiber samples, we assumed that after formation of one monolayer, the rest of the adsorbed vapor film could be considered as liquid and therefore we

integrated only to one theoretical adsorbed monolayer to determine π_{sv}. Based on obtained values of π_{sv}, the work of adhesion, W_A, was estimated:

$$W_A = 2\gamma_L + \pi_{SV} \quad (10)$$

When the work of adhesion of the water and ethanol are known, it is possible to estimate the dispersive and polar components of surface energy using Equations 4 and 5.

2.5. Molecular modelling

The DFT simulations were made using the all electron atomic orbital based DFT code, DMol [43, 44]. We used the Perdew, Burke and Erzenhof (PBE) exhange-correlation functional [45] of the generalized gradient approximation type, along with a double numerical basis set with polarization. To describe the weak dispersion interaction that could arise, we used the Grimme dispersion correction [46]. All the calculations were performed at the Gamma point. The electronic convergence was set to 2.7×10^{-4} eV, geometries were converged to 10^{-4} Å and force convergence was set to 2.7×10^{-2} eV/Å.

The *ab initio* molecular dynamics (MD) simulations were performed for 11 ps with a time step of 1 fs in a canonical ensemble (NVT) at 400 K and 600 K. These temperatures were chosen both to help overcome energy barriers in the potential energy surface and to simulate the elevated temperatures seen in actual experiments.

The α-quartz surface was created from an experimentally determined bulk structure by Levien et al. [47]. We produced a {00.1} face and constructed a [2 × 2] supercell containing 5 layers of silicon. The middle layers were fixed at their bulk positions, while both hydrogen passivated surfaces were allowed to relax. The resulting cell parameters were 9.82 Å × 10.80 Å × 31.48 Å, which includes at least 20 Å of vacuum spacer. The APS molecule was placed on this quartz surface in two orientations, with the amino group facing the quartz surface and with the silanol group facing the quartz surface. We reported the minimum energy configuration for these orientations in a previous study [5]. Here, we used these configurations as our starting structures for the *ab initio* molecular dynamics simulations. To simulate humidity, we randomly placed 10 water molecules around the APS molecule.

3. Results and discussion

3.1. Characterization of initial materials

We characterized surface composition, area, charge and wettability of untreated wafers (U-Si, U-SWM), fibers (U-SWF) and APS treated wafers (Si-APS, SWM-APS) and fibers (SWF-APS) as well as commercially available fiber materials containing APS and oil (SWF-APS-Oil), oil (SWF-Oil) and PUF binder (SWF-PUF). The full surface composition, derived from XPS, is presented as Table S1 in Supporting Information. In Table 2, we show the carbon content and the N/Si and C/Si surface concentration ratios, which indicate the presence of APS [48] and other organic matter such as oil and PUF. As expected, the surface concentration of carbon and the C/Si ratio are significantly higher for samples treated with APS, and especially where oil or PUF were applied (SWF-APS-Oil, SWF-Oil, SWF-PUF). The use of oil in fiber production increases fiber hydrophobicity, making the material water repellent, thus protecting the APS layer from the decomposition.

To characterize wetting behavior, we used contact angle measurements for wafers (Table S2, Supporting Information) and vapor adsorption for fibers. The surface energy results are listed in Table 2. Generally, the surface energies from the contact angles for the wafers were significantly lower than those determined with vapor adsorption for the fibers. This can be explained by the differences in the techniques. For calculating surface energy with contact angles, the work of adhesion, W_A is limited to $2\gamma_L$, while there is no such limit in the vapor adsorption method, where W_A is found through integrating the adsorption isotherm. Differences in samples surface roughness can be another explanation for the observed differences. Silicon wafers (U-Si) used in this work are

chemically polished to the final surface roughness <2 Å, while untreated stone wool melt wafers (U-SWM) are mechanically polished, thus with expected higher surface roughness. Higher surface roughness leads to lower contact angle in case of good wetting, which is observed as lower water contact angle on U-SWM than on U-Si. Fiber surface roughness, U-SWF, can be significantly different from wafers, because of the differences in production methods, where fibers are expected to have smoother surface than mechanically polished wafers. Moreover, surface roughness of the stone wool materials (both wafers and fibers) can significantly increase upon interaction with humidity at elevated temperatures, because of the leaching of network modifiers cations [49],[50] and network formers [7]. Treatment with APS increases surface roughness of fibers [51] and wafer materials [5], while PUF binder is preferably distributed as micrometer-size discrete droplets on stone wool fibers [52].

Table 2. Surface composition, area, charge and wettability of all investigated materials[§].

Samples	Wafers				Fibers				
					untreated	treated in the lab	treated at industry scale		
	U-Si	Si-APS	U-SWM	SWM-APS	U-SWF	SWF-APS	SWF-APS-Oil	SWF-Oil	SWF-PUF
	Surface area, m^2/g								
	-	-	-	-	0.3	0.2	0.2	0.2	0.1
	XPS intensity ratios								
% C	4.5±0.3	13.4±1.0	9.7±0.1	39.9±8.3	14.7±0.4	24.1±10.7	47.7±4.1	35.2±0.4	88.3
N/Si	0	0.04±0.001	0.04±0.01	0.34±0.11	0.05±0.01	0.25±0.10	0.11±0.03	0	0.6
C/Si	0.11±0.01	0.36±0.04	0.52±0.01	2.6±1.1	1.0±0.1	1.6±1.1	3.8±0.6	2.8±0.1	40.1
	IEP, pH units								
	<3.0	8.2	2.7 – 3.2	8.5	4.5	10.3	10.1	4.7	4.5
	Wettability								
H_2O contact angle, °	14.4±0.5	61.7±1.7	8.2±2.4	74.1±5.9	-	-	-	-	-
Total surf. energy γ_s, mJ/m^2	75.9*	52.8*	76.5*	43.6*	265.9**	201.8**	153.3**	164.5**	153.1**
Dispersive surf. energy, γ_d, mJ/m^2	42.6*	42.1*	41.0*	37.4*	40.8**	7.6**	6.4**	30.2**	4.6**
Polar surf. energy, γ_p, mJ/m^2	33.3*	10.7*	35.5*	6.2*	225.1**	194.2**	146.9**	134.3**	148.5**
$\gamma_{sw} - \gamma_{so}$, mJ/m^2	-46.3*	8.8*	-50.2*	14.5*	-	-	-	-	-
Max. H_2O ads.,*** mg/m^2	-	-	-	-	5	11	3	1	12

§ XPS and IEP data for U-Si, U-SWM, Si-APS, SWM-APS, U-SWF are compiled from Okhrimenko et al. 2017 [5], XPS and IEP data for SWF-PUF are compiled from Okhrimenko et al., 2018 [6]

* from diiodomethane-water and water in n-dodecane contact angle measurements.

** from water and ethanol vapor adsorption at 293 K and 1 monolayer coverage.

*** from vapor adsorption at $P/P_0 = 0.9$ and 293 K

Despite method and surface roughness differences, the obtained trends for wafers and fibers are quite similar. The results of the water contact angle measurements and the surface energy determinations for the wafers are consistent with literature data [53-56]. The untreated samples (U-Si, U-SWM, U-SWF) had higher surface energy than after treatment with APS (Si-APS, SWM-APS, SWF-APS). The highest surface energy decrease was observed for fiber samples containing organic material, oil and PUF (SWF-APS-Oil, SWF-Oil, SWF-PUF). The polar and dispersive components of surface energy (Figure 1a,b) showed that the overall decrease of surface energy resulted mostly from the decrease of the polar component. This was also observed with inverse gas chromatography [57]. In this work, the decrease correlates well with the amount of organic matter in the samples, which is represented as surface carbon composition (Figure 1).

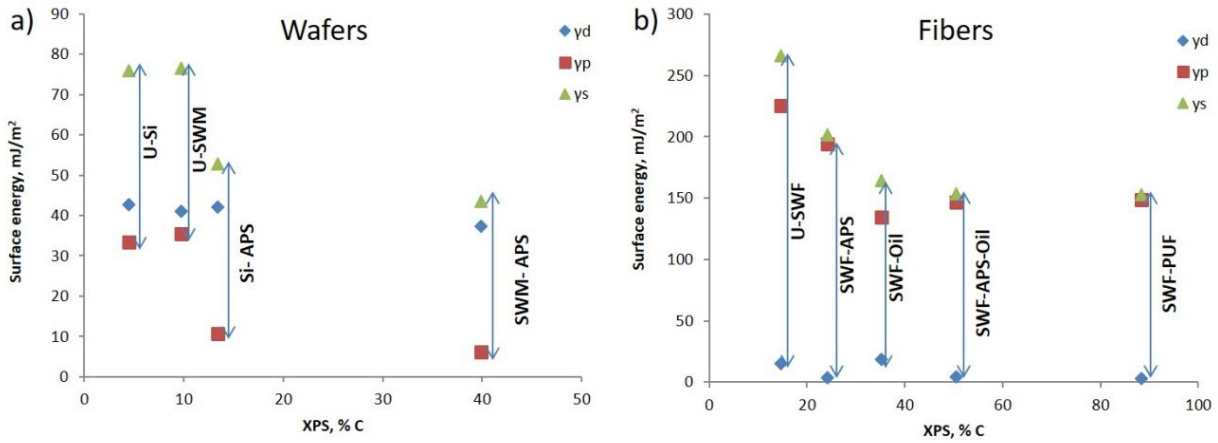

Figure 1. The dependence of dispersive (γd), polar (γp) and total (γs) surface energy on the surface concentration of carbon measured with XPS for a) wafers, determined with diiodomethane and water contact angle and b) fibers, determined with water and ethanol vapor adsorption.

Further insight into wettability can be derived from preferential wetting results. For wafers, we estimated preferential wetting by measuring water contact angle in n-dodecane and calculating the interfacial surface tension between solid – water, γ_{SW}, and solid – n-dodecane, γ_{SO} (Table 2). Treatment with APS increases γ_{SW} and decreases γ_{SO}, making their difference positive compared with negative values for the untreated U-Si and U-SWM. When $\gamma_{SW} - \gamma_{SO}$ is positive, the surface is oil wet; when $\gamma_{SW} - \gamma_{SO}$ is negative, the surface is water wet. Wafer surface wettability turns from water to oil wet with increased surface carbon, which mostly results from APS treatment.

For fiber materials, analysis of preferential wettability was made using the isosteric heat of adsorption for water and ethanol. This method does not require liquids to be immiscible, as in contact angle analysis, because the effect of each liquid is measured separately. We chose ethanol [41] to represent the organic phase and compared its heat of adsorption with that of water. Figure 2 presents the dependence of isosteric heat of adsorption on surface coverage for all fiber materials, where the reference lines for heat of liquefaction for water and ethanol are also shown. If the adsorption energy profile is above the reference line, then the surface is wetted by that vapor (liquid). At high coverage, the adsorption energy profile normally seeks the reference liquefaction line, because only interaction between adsorbate molecules can happen and no more interaction between the solid surface and vapor molecules is possible.

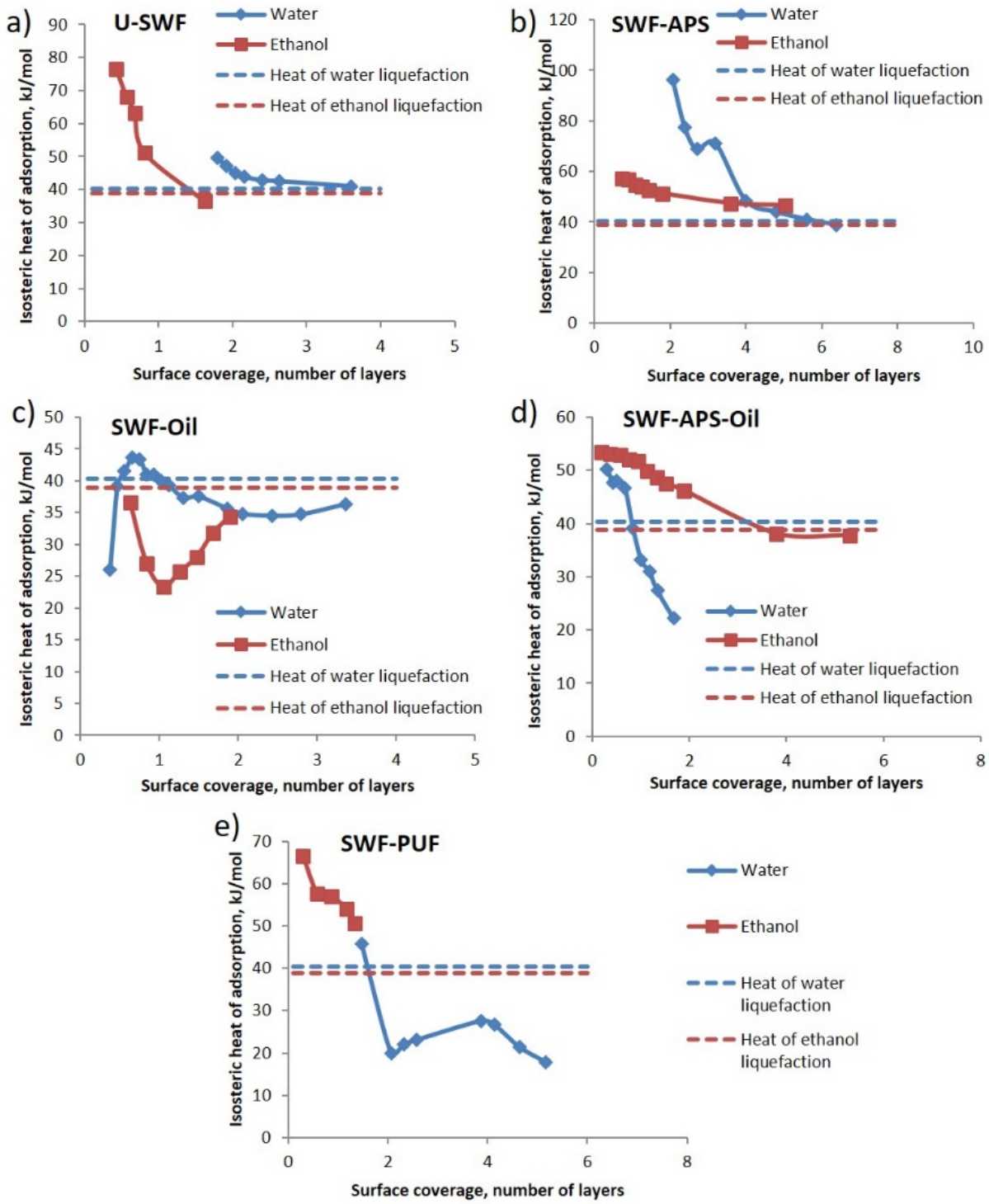

Figure 2. The dependence of isostreic heat of water and ethanol adsorption on surface coverage for a) U-SWF, b) SWF-APS, c) SWF-Oil, d) SWF-APS-Oil, e) SWF-PUF.

To determine preferential wetting, the energy profiles for water and ethanol were compared. For U-SWF and SWF-APS, the water energy profile is higher than for ethanol, thus we can expect these samples to be preferentially water wet. We also observed an increase in heat of water adsorption for SWF-APS compared with U-SWF, consistent with previous work [58]. This probably results from high affinity of the amino groups for water molecules. Samples that contain high amounts of organic matter showed different behavior. For SWF-APS-Oil and SWF-PUF samples, the ethanol energy profile is higher than water, thus these samples are more oil wet. For the SWF-Oil sample,

both water and ethanol energy profiles are very close to their liquefaction reference lines, showing weak surface affinity with both molecules, thus also hydrophobic character.

Despite the different wetting properties of the fiber samples, their total amount of water adsorbed (Table 2) is quite high. This shows that after the first few molecular water layers are formed, the fiber samples can still attract a significant amount of water. The decrease in surface energy, especially its polar component, and low water isosteric heat of adsorption should indicate decrease of water wetness and thus decrease of water uptake. However, this is only true for SWF-Oil and SWF-APS-Oil compared with U-SWF. For SWF-APS and SWF-PUF, the water uptake is higher than for U-SWF. For SWF-Oil, SWF-APS-Oil and SWF-PUF, the high water uptake can be explained by condensation of vapor between the fibers, rather than only on their surfaces. For SWF-APS, the analysis of the isosteric heat of adsorption data showed that this sample is quite hydrophilic. This is consistent with the contact angle study performed on the fiber melt wafers treated with APS, SWM-APS, which had similar chemical composition. SWM-APS is close to mixed wet, with water contact angle in air and in n-dodecane of 74 and 106°.

It was previously shown [5, 6, 14, 24], that moisture can influence the stability of APS and PUF binder, especially at elevated temperatures. Fiber surface morphology can also be influenced by increased temperature and humidity [49] and increase of stone wool fibers surface roughness was observed [50]. The water contact angle for the APS treated silica and the fiber melt wafers in air also showed that these surfaces are close to mixed wet. Only when an organic phase is present (e.g. n-dodecane), can water be displaced from the surface. Fiber materials adsorb relatively high amounts of water, in spite of their surface energy and wetting properties. To investigate the relationship between wettability and the stability of APS and PUF treatments on fibers and wafers, we performed ageing experiments over a wide range of temperature and humidity.

3.2. Ageing

We investigated the effects of ageing, using surface concentration ratios for N/Si and C/Si and streaming potential for isoelectric point (IEP) for Si-APS, SWM-APS, SWF-APS, SWF-APS-Oil and SWF-PUF. For U-SWF and SWF-Oil, we made analyses only after ageing for 21 days at 70 °C and 91% RH. We also made water adsorption experiments for these samples (Table 3). There was no significant difference for the U-SWF sample after ageing. A slight increase in IEP and the C/Si ratio and decrease in the amount of adsorbed water can be explained sample inhomogeneity and by organic carbon contamination from the air during ageing. In contrast, the SWF-Oil sample apparently lost some organic material during ageing. The IEP and C/Si ratio decreased, and water uptake increased after ageing for 21 days at 70 °C and 91% RH.

Table 3. Change in wettability and composition after ageing at 70 °C and 91% RH for 21 days.

Sample	U-SWF		SWF-Oil	
Days of ageing	0	21	0	21
IEP, pH units	4.5	4.7	4.7	4.2
XPS C/Si	1.0±0.1	1.2±0.1	2.8±0.1	2.4±0.1
Number of adsorbed water layers	21	19	5	8

The results of the isoelectric point (IEP) determination for Si-APS, SWM-APS, SWF-APS, SWF-APS-Oil and SWF-PUF are shown by Figures 3. For the samples with APS, the initial IEP for unaged samples was at high pH because of the basic nature of APS amino groups, consistent with earlier observations [51, 59, 60]. For the unaged SWF-PUF sample, the IEP was at pH 4.5, a typical value for polymers with no functional groups [61]. When APS or PUF binder decompose during ageing, IEP shifts toward the acidic region [5, 6], reflecting more acidic –SiOH, from the substrate,

which becomes available, as the APS, PUF or oil are removed. The decline of IEP depends on ageing conditions (temperature and humidity), the initial amount of APS and on the substrate itself.

For SWM-APS, fast decrease of IEP to pH 4.6 was observed for all investigated ageing conditions, except for the mildest, i.e. room temperature and 55% RH (Figure 3b). From our previous investigations [5], the IEP at pH 4.0 indicates that less than 5% of the surface remains covered with the APS coupling agent. APS deposited on silica wafers (Figure 3a) was more stable towards ageing at room and slightly elevated temperatures (50 °C) but IEP dropped toward pH 4.0 after 7 days of ageing at 70 °C or after 3 hours in the water bath at 80 °C, indicating full APS layer decomposition.

SWF-APS showed IEP at high pH (10.3) for the unaged material because the sample preparation leaves all of the APS on the fibers (Figure 3c). During ageing under mild conditions at room temperature, no decrease of IEP was observed. In contrast, IEP increased slightly for samples aged at room temperature and 97% RH, which is explained by swelling or rearranging of the APS layers. The decomposition of APS layers starts only at elevated temperatures, 50 and 70 °C. At 70 °C, ageing is faster at 91% than at 75% RH. After 14 days ageing at 70°C/91% RH, decomposition of the APS layers is more significant than after ageing in a water bath at 80 °C for 3 hours. After 28 days of ageing at 70°C/91% RH, the IEP drops to pH 4.0, indicating full decomposition of the APS layers. For the unaged SWF-APS-Oil, the IEP is at pH 10.1, similar to SWF-APS (Figure 3d). However, the ageing behavior of SWF-APS-Oil is significantly different that for SWF-APS. SWF-APS-Oil contains oil, that prevents water penetration to the surface, which would hydrolyze the Si-O-Si bonds between the APS and the surface. Therefore, under similar conditions of ageing, SWF-APS-Oil progresses more slowly than SWF-APS. No difference in IEP was observed for SWF-APS-Oil samples aged for 28 days at room temperature and 55 and 97% relative humidity, compared with unaged SWF-APS-Oil. At higher temperatures, the APS layer begins to decompose, and the effect is more pronounced at 70 °C than at 50 °C. At 70 °C there is no difference between ageing at 75% and 91% relative humidity. Based on these results, we conclude that temperature has a stronger influence on the decomposition of APS layers than relative humidity. After 7 days of ageing at 70 °C, the degree of APS layer decomposition is similar to that seen after ageing for 3 hours at 80 °C in a water bath.

The dependence of IEP on ageing conditions for SWF-PUF is shown by Figure 3e. Ageing at 50 °C/95% RH and 70 °C/91% RH for 7 days is more harsh than ageing in a water bath at 80 °C for 3 hours. We point out that because SWF-PUF and SWF-APS-Oil both contain oil, the samples do not completely wet in the water bath. Another interesting detail is that ageing at 70 °C/75% RH has a similar effect to ageing at room temperature/97% RH. In contrast to SWF-APS-Oil, where temperature has a higher impact on ageing than humidity, for PUF ageing, the relative humidity level is more determinant than the ageing temperature. Previously [52], it was shown that PUF binder is preferentially located as discrete droplets of micrometer size on stone wool fibers, and thin 4 nm organic layer on the fiber surface was predicted by QUASES-XPS analysis [6]. The decrease of IEP can be thus explained by the partial removal of this layer, because micrometer size binder droplets are expected to be quite stable [52].

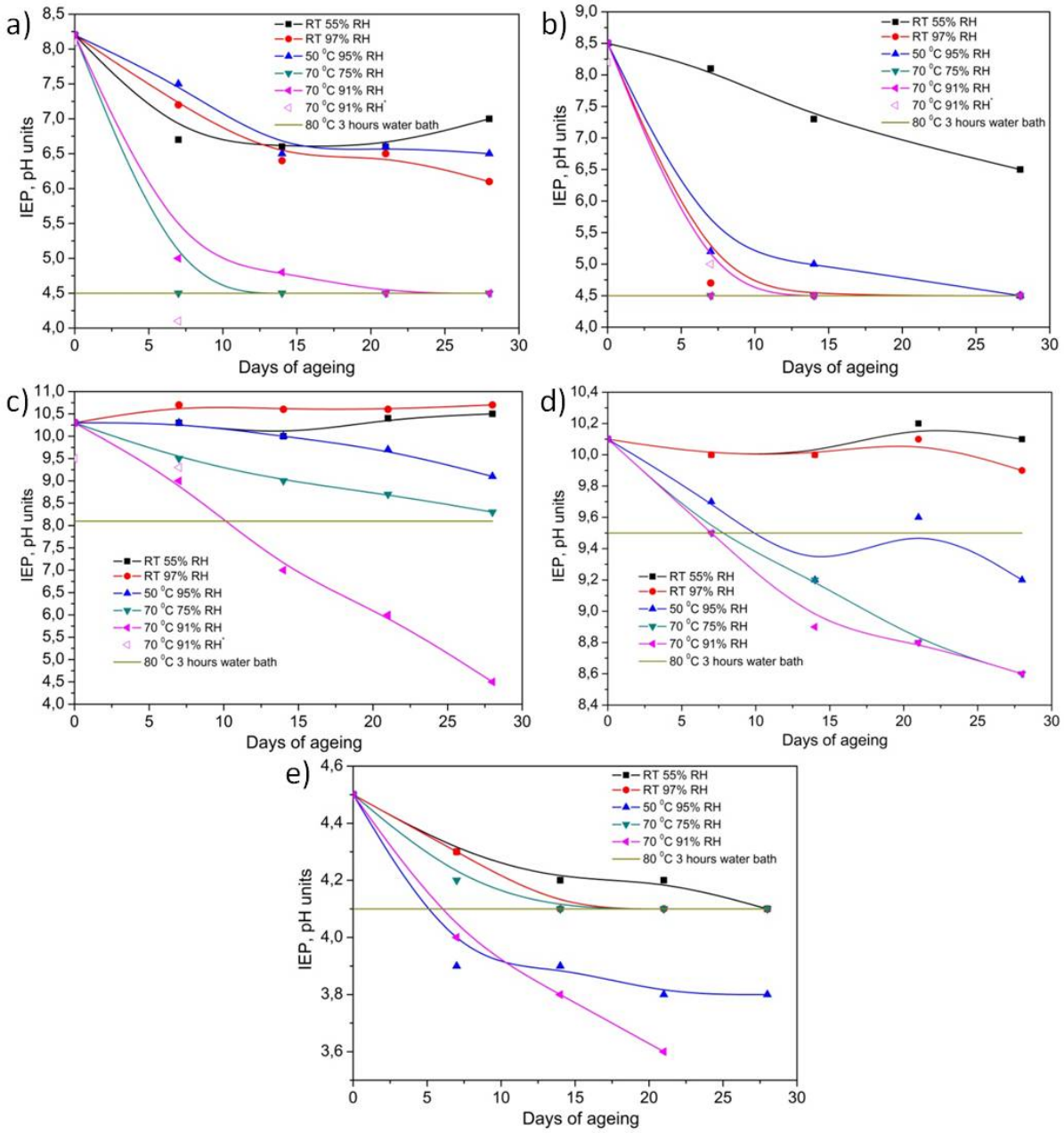

Figure 3. The dependence of the isoelectric point (IEP) on ageing time, temperature and relative humidity for a) Si-APS; b) SWM-APS; c) SWF-APS; d) SWF-APS-Oil; e) SWF-PUF. The IEP after ageing in a water bath at 80 °C for 3 hours are shown as a reference line because this type of ageing is expected to be most harsh. For comparison, results at 70 °C and 91 % RH from Okhrimenko et al., 2017 [5] are included for a to c, as open triangles. For the SWF-PUF sample, data for the samples that are unaged, aged in water bath and aged at 70°C and 91% RH for 7 days are compiled from Okhrimenko et al., 2018 [6].

XPS results are presented in Figure 4. Element ratios were chosen specifically, to follow change in surface composition caused by ageing; which depends on the system under consideration. Previously [5], the N/Si ratio was used for tracking change during ageing because it works well for systems containing APS. Nitrogen is a key component in amines and the Si signal mainly comes from the substrate [62]. Therefore, decrease in the N/Si ratio directly relates to decomposition or loss of adsorbed APS. The APS ageing behavior for the SWF-APS sample depends on temperature and humidity (Figure 4a) and XPS results agree well with the IEP. The fastest decrease of N/Si was observed when fibers were aged at 70 °C/91% RH. After 7 days the N/Si ratio was equal to the ratio after water bath ageing for 3 hours at 80 °C. The milder the ageing conditions, the lower the

decrease of N/Si, thus less decomposition of APS layer. When SWF-APS was aged at room temperature and high humidity (97% RH), the N/Si increased. This parallels a slight increase of the IEP for the same samples (Figure 3c) and can indicate swelling and rearrangement of the APS layers, exposing more amino groups, rather than decomposition. The N/Si change with ageing is more complicated for SWF-APS-Oil (Figure 4b). There was minimal change for samples aged at room temperature, which correlates well with IEP determinations (Figure 3d). However, ageing at elevated temperatures and in the water bath, promoted increased N/Si and decreased IEP. One explanation is that oil prevents water penetration into the fiber samples, so the APS layers hydrolyze and probably swell, as for the SWF-APS samples, but detached APS molecules remain close to the fiber surface. When a stream of liquid is applied in zeta potential experiments, these fragments are removed from the fiber, leaving the bare surface behind, thus decreasing IEP. In XPS experiments, where analysis is conducted in vacuum, such flushing is impossible, so swelled APS layers increase the surface concentration of nitrogen, thus increases the N/Si ratio.

For SWF-PUF, where the carbon signal from PUF and oil dominates the XPS spectra, we used the C/Si ratio (Figure 4c) instead of N/Si. C/Si for SWF-PUF samples drops with ageing and the harsher the ageing conditions, the faster the decrease. However, by using C/Si ratio, it is not possible to distinguish between oil and binder removal from the surface. The decrease of C/Si ratio for SWF-PUF can be connected with removal of thin 4 nm organic layer [6] from the fiber surface, which would also lead to IEP shift towards lower pH. XPS C/Si for SWF-PUF was still high after ageing under all investigated conditions, which indicates that major fraction of PUF binder remained on the fiber surface, in the form of discrete micrometer-size droplets [52]. XPS interpretation difficulties for the SWF-PUF and SWF-APS-Oil can arise from their complex nature, i.e. many components, but the IEP data complement the XPS results, giving a better perspective for these samples.

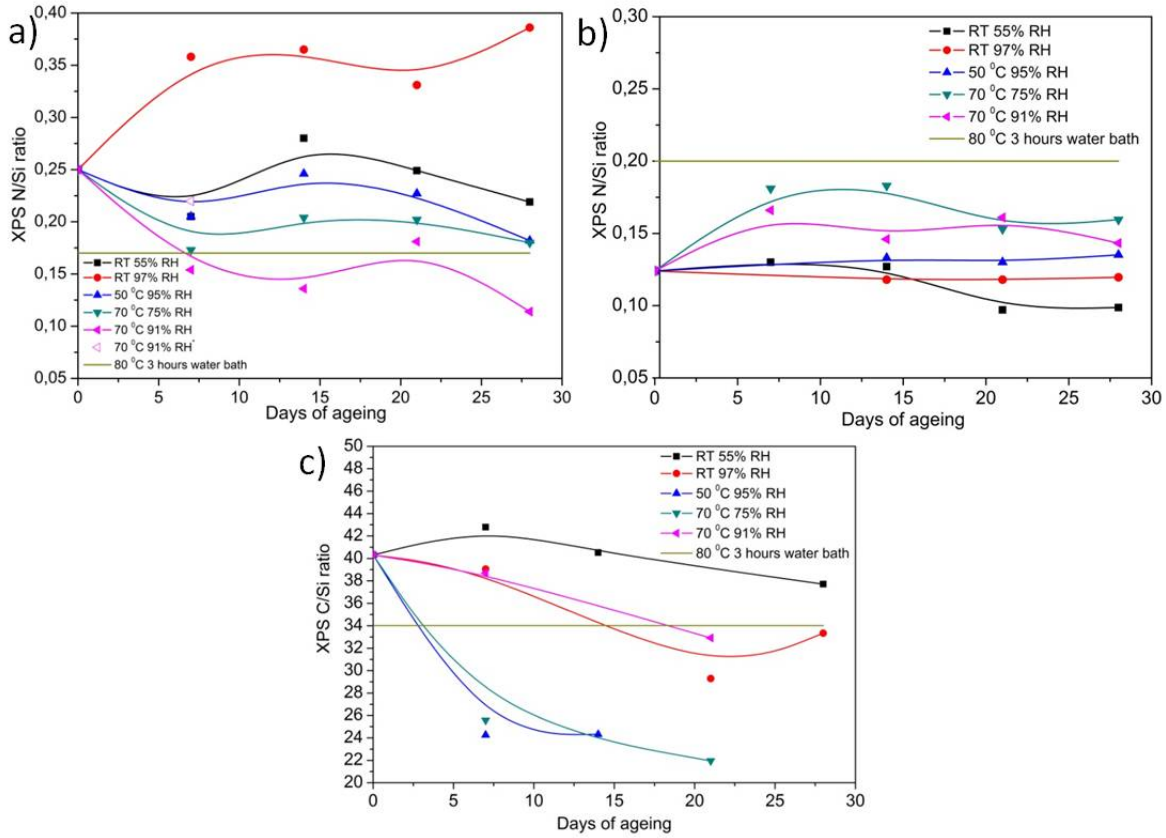

Figure 4. The dependence of XPS N/Si ratio on ageing time and conditions for a) SWF-APS, b) SWF-APS-Oil and the dependence of XPS C/Si ratio on ageing time and conditions for c) SWF-PUF. The N/Si and C/Si ratios, after ageing in a water bath at 80 °C for 3 hours, are shown as

reference lines, because this type of ageing is expected to be the harshest. For comparison, the result at 70 °C and 91 % RH from Okhrimenko et al., 2017 [5] is shown for SWF-APS as an open triangle. For the SWF-PUF sample, the values for samples that are unaged, aged in water bath and aged at 70°C and 91% RH for 7 days are compiled from Okhrimenko et al., 2018 [6].

Ageing results correlate well with the amount of water adsorbed by the fiber sample and to some extent with their hydrophilic-hydrophobic properties. SWF-APS is significantly more hydrophilic and adsorbs more water than SWF-APS-Oil and this is the reason why APS layers are less stable for SWF-APS than for SWF-APS-Oil during exposure to high temperature and humidity. However, at room temperature, there was no sign of APS layers decomposition. Therefore, we conclude that temperature plays a more important role in the decomposition mechanism for APS layers. The SWF-PUF sample can adsorb significant amounts of water and for this sample, increased humidity accelerates organic layer degradation faster than if only the temperature is increased. This is in accordance with the low isosteric heat of water adsorption for this sample. In fact, low isosteric heat of adsorption means that the amount of adsorbed water does not change much in the examined temperature range.

3.3 Theoretical simulations

To help explain the mechanism behind temperature and humidity effects on APS treated surfaces, we performed 11 ps *ab initio* MD simulations of APS on hydroxylated {00.1} quartz. Table 4 shows the final molecular structure from the simulations and Figure 5 shows the pair distribution function between APS and quartz, averaged over the entire simulation trajectory. For the starting configurations, where the amino group faces the quartz surface, increased temperature and addition of water minimally affects the structure, which is supported by the minimal change in the pair distribution function. However, for the starting configuration, where the silanol group is facing the quartz surface, the elevation in temperature alone stabilizes the APS by allowing the amino group of APS to form a bond with the quartz surface. This is shown as the large peak in the pair distribution function at around 1 Å. In the presence of water (increased humidity), the amino group is unable to attach itself to the surface. This potentially allows APS to be desorbed more easily. This is consistent with our observations that APS on silica wafers is less stable in a water bath.

Table 4. Structures predicted from *ab initio* MD calculations. Silicon atoms are shown in yellow, oxygen in red, nitrogen in blue, carbon in cyan and hydrogen in white. Hydrogen bonding is shown as dotted orange cylinders.

	Amino group facing quartz		Silanol group facing quartz	
	400 K	600 K	400 K	600 K
No water	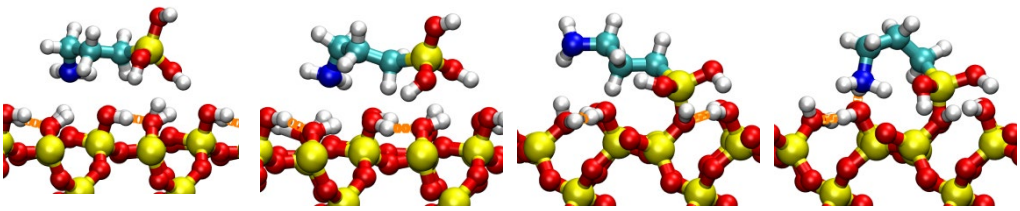			
10 water molecules	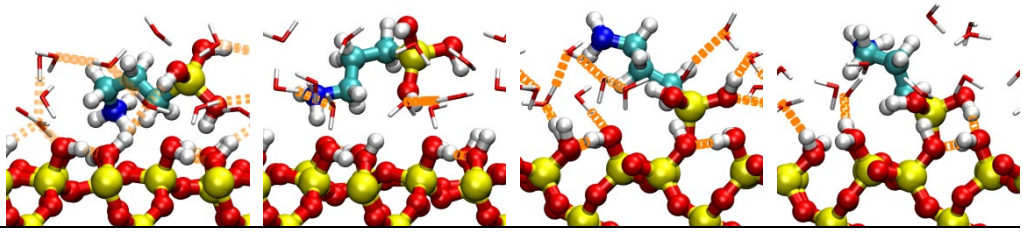			

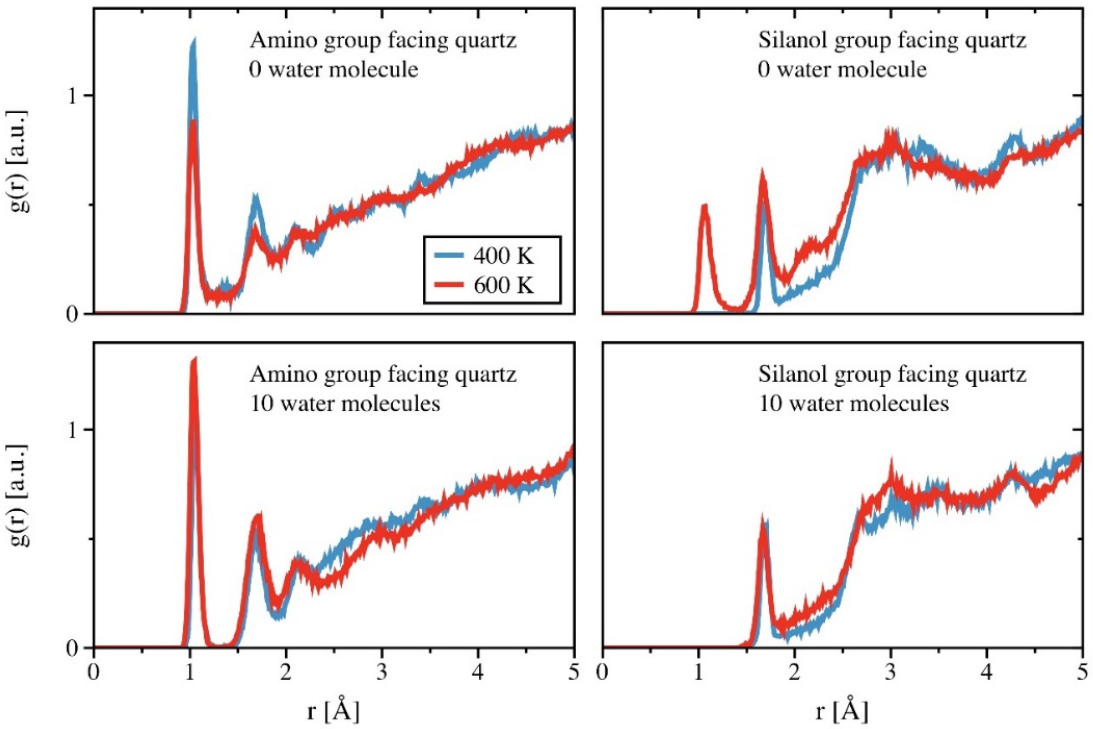

Figure 5. Pair distribution function between APS and quartz at 400 K and 600 K, averaged over the whole simulation trajectory.

Figure 6 shows the evolution in the number of hydrogen bonds for the systems studied here and Table 5 shows the number of hydrogen bonds for each system, averaged over the last 5 ps of the trajectory. The systems with a silanol group facing quartz have a smaller number of hydrogen bonds than the systems with an amino group facing quartz. This is because APS in the former system is covalently anchored on quartz, in contrast with anchoring by hydrogen bonding in the latter system. On average, the system with amino group facing quartz has 1.08 hydrogen bonds, arising from the amino group itself and the hydroxylated quartz surface. Increase in temperature destabilizes the bond, causing the number to decrease to 0.77. On the other hand, increasing the humidity increases this number to 1.30, which corresponds to hydrogen bonds forming between APS and water. The fractional number reflects the mobility of the water molecules around the APS. Some of these hydrogen bonds are lost at increased temperature, with the number dropping to 1.12. Increasing the temperature for the system with a silanol group facing quartz increases the number of hydrogen bonds from 0.06 to 0.13. This correlates with the amino group twisting, to come into close contact with the quartz surface. At increased humidity, the average number of hydrogen bonds is 0.96, which comes only from interaction between APS and the water molecules. This is supported by the pair distribution function (Figure 5), which shows the lack of a characteristic peak at ~1 Å, that is associated with hydrogen bonding between the amino group of APS and the quartz surface. At elevated temperature, the number of hydrogen bonds drops to 0.28 and is directly correlated with increased water molecule mobility.

Table 5. Average number of hydrogen bonds between APS and other components (quartz and water molecules) over the last 5 ps of the simulation trajectory.

	Amino group facing quartz		Silanol group facing quartz	
	400 K	600 K	400 K	600 K
No water	1.08	0.77	0.06	0.13
10 water molecules	1.30	1.12	0.96	0.28

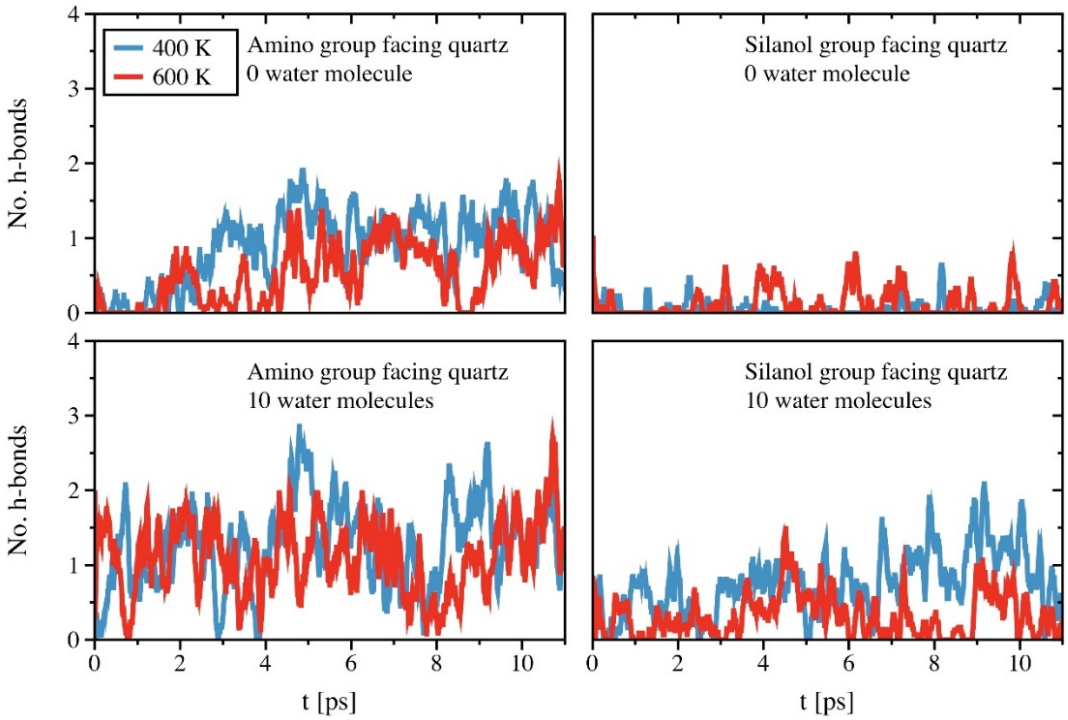

Figure 6. Number of hydrogen bonds between APS and other components (quartz and water molecules) over the simulation trajectory, plotted with a 0.1 ps moving average.

4. Conclusions

We investigated how the wettability of silicate materials treated with APS coupling agent and PUF binder influences their hydrolytic stability. Treating with APS reduces the hydrophilic properties of silicate materials and the surface becomes more mixed wet. The methods for determining surface energy and wettability through contact angle and vapor adsorption showed different results for wafer and fiber materials but we found a similar trend for a decreasing polar component of surface energy when APS, PUF or oil treatment are applied to the sample. Despite this decrease, the application of only APS and PUF to the silicate surface is not enough to create water repellent layers of coupling and binder agents. Water vapor can still adsorb on the surface and react at the APS-silicate interface, hydrolyzing Si-O-Si bonds and destroying the APS layer. The *ab initio* MD simulations suggested a possible mechanism by which APS-silicate bonds are degraded. Thinner layers of APS deposited on silicate wafer surface by dipping are less stable than the multilayers that result on fibers. However, at elevated temperature and humidity, an extra hydrophobic protection, such as treating with oil, is required to keep the APS coupling agent layers stable. This helps to reduce the degradation rate of the APS coupling agent layers and keep them reactive toward further treatment with organic binder. Fiber materials containing PUF binder also suffer, however to less extent, from reaction with water vapor, because water uptake of these materials is high and quite insensitive to temperature change.

Determination of the isoelectric point (IEP) for the fiber and wafer silicate materials, can be used for the APS and PUF stability, as well as for APS layer reactivity investigations, where different agents for increasing hydrophobic properties of the material are applied. Further search for agents that increase hydrophobicity, thus preventing reaction of APS and PUF with water, is necessary to create materials that are more stable in terms of resisting ageing at elevated humidity and temperatures.

Acknowledgments
We thank Jesper Matthiesen for help with the contact angle apparatus and Keld West for general lab support. The funding was provided by Innovation Foundation, Denmark and ROCKWOOL International A/S. Comments from anonymous reviewer are greatly appreciated.

Supporting Information
XPS data for material characterization and contact angle measurements are available online free of charge.

References
[1] J.L. Thomason, Glass fibre sizing: A review, Composites Part A: Applied Science and Manufacturing 127 (2019) 105619.

[2] Y. Xie, C.A. Hill, Z. Xiao, H. Militz, C. Mai, Silane coupling agents used for natural fiber/polymer composites: A review, Composites Part A: Applied Science and Manufacturing 41(7) (2010) 806-819.

[3] A. Miller, J. Berg, Effect of silane coupling agent adsorbate structure on adhesion performance with a polymeric matrix, Composites Part A: Applied Science and Manufacturing 34(4) (2003) 327-332.

[4] S. Kowatsch, Mineral Wool Insulation Binders, in: L. Pilato (Ed.), Phenolic Resins: A Century of Progress, Springer Berlin Heidelberg, Berlin, Heidelberg, 2010, pp. 209-242.

[5] D.V. Okhrimenko, A. Budi, M. Ceccato, M. Cárdenas, D.B. Johansson, D. Lybye, K. Bechgaard, M.P. Andersson, S.L. Stipp, Hydrolytic stability of 3-aminopropylsilane coupling agent on silica and silicate surfaces at elevated temperatures, ACS applied materials & interfaces 9(9) (2017) 8344-8353.

[6] D.V. Okhrimenko, A.B. Thomsen, M. Ceccato, D.B. Johansson, D. Lybye, K. Bechgaard, S. Tougaard, S.L.S. Stipp, Impact of curing time on ageing and degradation of phenol-urea-formaldehyde binder, Polymer Degradation and Stability 152 (2018) 86-94.

[7] D.V. Okhrimenko, C.F. Nielsen, L.Z. Lakshtanov, K.N. Dalby, D.B. Johansson, M. Solvang, J. Deubener, S.L.S. Stipp, Surface reactivity and dissolution properties of alumina-silica glasses and fibers, ACS Applied Materials & Interfaces (2020).

[8] H. Min, P.-L. Girard-Lauriault, T. Gross, A. Lippitz, P. Dietrich, W.E. Unger, Ambient-ageing processes in amine self-assembled monolayers on microarray slides as studied by ToF-SIMS with principal component analysis, XPS, and NEXAFS spectroscopy, Analytical and bioanalytical chemistry 403(2) (2012) 613-623.

[9] E.T. Vandenberg, L. Bertilsson, B. Liedberg, K. Uvdal, R. Erlandsson, H. Elwing, I. Lundström, Structure of 3-aminopropyl triethoxy silane on silicon oxide, Journal of Colloid and Interface Science 147(1) (1991) 103-118.

[10] J. Kim, P. Seidler, C. Fill, L.S. Wan, Investigations of the effect of curing conditions on the structure and stability of amino-functionalized organic films on silicon substrates by Fourier transform infrared spectroscopy, ellipsometry, and fluorescence microscopy, Surface Science 602(21) (2008) 3323-3330.

[11] R.M. Pasternack, S. Rivillon Amy, Y.J. Chabal, Attachment of 3-(aminopropyl) triethoxysilane on silicon oxide surfaces: dependence on solution temperature, Langmuir 24(22) (2008) 12963-12971.

[12] E. Asenath Smith, W. Chen, How To Prevent the Loss of Surface Functionality Derived from Aminosilanes, Langmuir 24(21) (2008) 12405-12409.

[13] M. Zhu, M.Z. Lerum, W. Chen, How To Prepare Reproducible, Homogeneous, and Hydrolytically Stable Aminosilane-Derived Layers on Silica, Langmuir 28(1) (2011) 416-423.

[14] A. Zafar, J. Schjødt-Thomsen, R. Sodhi, R. Goacher, D. Kubber, X-ray photoelectron spectroscopy and time-of-flight secondary ion mass spectrometry characterization of aging effects on the mineral fibers treated with aminopropylsilane and quaternary ammonium compounds, Surface and Interface Analysis 44(7) (2012) 811-818.

[15] A.R. Yadav, R. Sriram, J.A. Carter, B.L. Miller, Comparative study of solution–phase and vapor–phase deposition of aminosilanes on silicon dioxide surfaces, Materials Science and Engineering: C 35(0) (2014) 283-290.

[16] M. Etienne, A. Walcarius, Analytical investigation of the chemical reactivity and stability of aminopropyl-grafted silica in aqueous medium, Talanta 59(6) (2003) 1173-1188.

[17] D.F. Siqueira Petri, G. Wenz, P. Schunk, T. Schimmel, An Improved Method for the Assembly of Amino-Terminated Monolayers on SiO2 and the Vapor Deposition of Gold Layers, Langmuir 15(13) (1999) 4520-4523.

[18] G.G. Allan, J. Dutkiewicz, E.J. Gilmartin, Long-term stability of urea-formaldehyde foam insulation, Environmental Science & Technology 14(10) (1980) 1235-1240.

[19] P. Kavvouras, D. Koniditsiolis, J. Petinarakis, Resistance of cured urea-formaldehyde resins to hydrolysis: a method of evaluation, Holzforschung-International Journal of the Biology, Chemistry, Physics and Technology of Wood 52(1) (1998) 105-110.

[20] O. Ringena, R. Janzon, G. Pfizenmayer, M. Schulte, R. Lehnen, Estimating the hydrolytic durability of cured wood adhesives by measuring formaldehyde liberation and structural stability, Holz Roh Werkst 64(4) (2006) 321-326.

[21] Z.A. Abdullah, B.D. Park, Hydrolytic stability of cured urea-formaldehyde resins modified by additives, Journal of applied polymer science 114(2) (2009) 1011-1017.

[22] Y.-f. Zhang, C.-h. Yang, Y.-w. Li, L.-y. Liang, M.-g. Lu, Low formaldehyde emission urea-formaldehyde resins modified by 2, 4, 6-trimethylolphenate and physical properties of its impregnated papers, Journal of Polymer Research 21(3) (2014) 1-8.

[23] J. Kim, J.-H. Lee, S.-G. Jeong, S. Kim, Formaldehyde emissions from particle board made with phenol–urea–formaldehyde resin prepared by different synthesis methods, Journal of Adhesion Science and Technology (ahead-of-print) (2015) 1-14.

[24] A. Zafar, J. Schjødt-Thomsen, R. Sodhi, R. Goacher, D. de Kubber, Investigation of the ageing effects on phenol-urea-formaldehyde binder and alkanol amine-acid anhydride binder coated mineral fibres, Polymer degradation and stability 98(1) (2013) 339-347.

[25] A.Y. Fadeev, T.J. McCarthy, Trialkylsilane monolayers covalently attached to silicon surfaces: wettability studies indicating that molecular topography contributes to contact angle hysteresis, Langmuir 15(11) (1999) 3759-3766.

[26] A.Y. Fadeev, T.J. McCarthy, Self-assembly is not the only reaction possible between alkyltrichlorosilanes and surfaces: monomolecular and oligomeric covalently attached layers of dichloro-and trichloroalkylsilanes on silicon, Langmuir 16(18) (2000) 7268-7274.

[27] T. Jesionowski, A. Krysztafkiewicz, Influence of silane coupling agents on surface properties of precipitated silicas, Applied Surface Science 172(1–2) (2001) 18-32.

[28] A. CARRE, V. LACARRIERE, Study of surface charge properties of minerals and surface-modified substrates by wettability, Contact Angle, Wettability and Adhesion, Volume 4 4 (2006) 267.

[29] D. Kowalczyk, S. Slomkowski, M.M. Chehimi, M. Delamar, Adsorption of aminopropyltriethoxy silane on quartz: an XPS and contact angle measurements study, International Journal of Adhesion and Adhesives 16(4) (1996) 227-232.

[30] Z. Kessaissia, E. Papirer, J.-B. Donnet, The surface energy of silicas, grafted with alkyl chains of increasing lengths, as measured by contact angle techniques, Journal of Colloid and Interface Science 82(2) (1981) 526-533.

[31] J.-M.N. Park, J.H. Kim, Surface Energies of Borosilicate Glass Surfaces Modified with n-Alkyl Silane Coupling Agents via Dynamic Contact Angle Measurements, Journal of Colloid and Interface Science 168(1) (1994) 103-110.

[32] N. Kamisetty, S. Pack, M. Nonogawa, K. Devarayapalli, T. Kodaki, K. Makino, Development of an efficient amine-functionalized glass platform by additional silanization treatment with alkylsilane, Analytical and Bioanalytical Chemistry 386(6) (2006) 1649-1655.

[33] Y. Mo, M. Zhu, M. Bai, Preparation and nano/microtribological properties of perfluorododecanoic acid (PFDA)–3-aminopropyltriethoxysilane (APS) self-assembled dual-layer film deposited on silicon, Colloids and Surfaces A: Physicochemical and Engineering Aspects 322(1–3) (2008) 170-176.

[34] A. Menawat, H. Joseph Jr, R. Siriwardane, Control of surface energy of glass by surface reactions: Contact angle and stability, Journal of Colloid and Interface Science 101(1) (1984) 110-119.

[35] X. Song, J. Zhai, Y. Wang, L. Jiang, Self-assembly of amino-functionalized monolayers on silicon surfaces and preparation of superhydrophobic surfaces based on alkanoic acid dual layers and surface roughening, Journal of Colloid and Interface Science 298(1) (2006) 267-273.

[36] C. Van Oss, R. Good, M. Chaudhury, Additive and nonadditive surface tension components and the interpretation of contact angles, Langmuir 4(4) (1988) 884-891.

[37] D.K. Owens, R. Wendt, Estimation of the surface free energy of polymers, Journal of applied polymer science 13(8) (1969) 1741-1747.

[38] F.M. Fowkes, Additivity of intermolecular forces at interfaces. i. determination of the contribution to surface and interfacial tensions of dispersion forces in various liquids1, The Journal of Physical Chemistry 67(12) (1963) 2538-2541.

[39] S. Zeppieri, J. Rodríguez, A. López de Ramos, Interfacial tension of alkane+ water systems, Journal of Chemical & Engineering Data 46(5) (2001) 1086-1088.

[40] S. Brunauer, P.H. Emmett, E. Teller, Adsorption of Gases in Multimolecular Layers, Journal of the American Chemical Society 60(2) (1938) 309-319.

[41] D. Okhrimenko, K.N. Dalby, L. Skovbjerg, N. Bovet, J.H. Christensen, S.L.S. Stipp, The surface reactivity of chalk (biogenic calcite) with hydrophilic and hydrophobic functional groups, Geochimica et Cosmochimica Acta 128 (2014) 212-224.

[42] L.J. Schlangen, L.K. Koopal, M.A.C. Stuart, J. Lyklema, Wettability: thermodynamic relationships between vapour adsorption and wetting, Colloids and Surfaces A: Physicochemical and Engineering Aspects 89(2-3) (1994) 157-167.

[43] B. Delley, An all-electron numerical method for solving the local density functional for polyatomic molecules, The Journal of chemical physics 92(1) (1990) 508-517.

[44] B. Delley, From molecules to solids with the DMol 3 approach, The Journal of chemical physics 113(18) (2000) 7756-7764.

[45] J.P. Perdew, K. Burke, M. Ernzerhof, Generalized gradient approximation made simple, Physical review letters 77(18) (1996) 3865.

[46] S. Grimme, Semiempirical GGA-type density functional constructed with a long-range dispersion correction, Journal of computational chemistry 27(15) (2006) 1787-1799.

[47] L. Levien, C.T. Prewitt, D.J. Weidner, Structure and elastic properties of quartz at pressure, American Mineralogist 65(9-10) (1980) 920-930.

[48] J.L. Thomason, D.W. Dwight, The use of XPS for characterisation of glass fibre coatings, Composites Part A: Applied Science and Manufacturing 30(12) (1999) 1401-1413.

[49] M.D. Lund, Y.-Z. Yue, Influences of chemical aging on the surface morphology and crystallization behavior of basaltic glass fibers, Journal of Non-Crystalline Solids 354(12) (2008) 1151-1154.

[50] M. Lund, Tensile strenght of glass fibers, 2009.

[51] R. Plonka, E. Mäder, S. Gao, C. Bellmann, V. Dutschk, S. Zhandarov, Adhesion of epoxy/glass fibre composites influenced by aging effects on sizings, Composites Part A: Applied science and manufacturing 35(10) (2004) 1207-1216.

[52] S.H. Barly, D.V. Okhrimenko, M. Solvang, Y. Yue, S.L. Stipp, Dissolution of stone wool fibers with phenol-urea-formaldehyde binder in a synthetic lung fluid, Chemical research in toxicology 32(12) (2019) 2398-2410.

[53] J. Böhmler, L. Ploux, V. Ball, K. Anselme, A. Ponche, Necessity of a Thorough Characterization of Functionalized Silicon Wafers before Biointerface Studies, The Journal of Physical Chemistry C 115(22) (2011) 11102-11111.

[54] B.P. Binks, J.H. Clint, Solid Wettability from Surface Energy Components: Relevance to Pickering Emulsions, Langmuir 18(4) (2002) 1270-1273.

[55] L. Černe, B. Simončič, M. Željko, The influence of repellent coatings on surface free energy of glass plate and cotton fabric, Applied Surface Science 254(20) (2008) 6467-6477.

[56] D. Janssen, R. De Palma, S. Verlaak, P. Heremans, W. Dehaen, Static solvent contact angle measurements, surface free energy and wettability determination of various self-assembled monolayers on silicon dioxide, Thin Solid Films 515(4) (2006) 1433-1438.

[57] V. Dutschk, E. Mäder, V. Rudoy, Determination of polarity parameters for glass fibres by inverse gas chromatography: Some results and remarks, Journal of adhesion science and technology 15(11) (2001) 1373-1389.

[58] T. Jesionowski, A. Krysztafkiewicz, Preparation of the hydrophilic/hydrophobic silica particles, Colloids and Surfaces A: Physicochemical and Engineering Aspects 207(1–3) (2002) 49-58.

[59] C. Bellmann, R. Plonka, A. Caspari, K. Grundke, Investigation of competitive adsorption of fibre sizing components: possibilities of electrokinetics, Composite Interfaces 20(4) (2013) 279-286.

[60] E. Metwalli, D. Haines, O. Becker, S. Conzone, C.G. Pantano, Surface characterizations of mono-, di-, and tri-aminosilane treated glass substrates, Journal of Colloid and Interface Science 298(2) (2006) 825-831.

[61] R.-C. Zhuang, T. Burghardt, R. Plonka, J.-W. Liu, E. Mäder, Affecting glass fibre surfaces and composite properties by two stage sizing application, eXPRESS Polymer Letters 4(12) (2010).

[62] J.L. Thomason, L.J. Adzima, Sizing up the interphase: an insider's guide to the science of sizing, Composites Part A: Applied Science and Manufacturing 32(3–4) (2001) 313-321.